EurJOC European Journal of Organic Chemistry

FULL PAPER

DOI: 10.1002/ejoc.201300745

Synthesis, Photophysics, and Electrochemistry of Tetra(2-thienyl)ethylene (TTE) Derivatives

Alessandro Bolzoni,[a] Lucia Viglianti,[a] Alberto Bossi,[b] Patrizia R. Mussini,[a] Silvia Cauteruccio,[a] Clara Baldoli,*[b] and Emanuela Licandro*[a]

Keywords: Cross-coupling / Fluorescence / Electrochemistry / Sulfur heterocycles / Solid-state emission

We have synthesized a series of tetra(2-thienyl)ethylene (TTE) derivatives, selectively functionalized at the thiophene α positions, either by a coupling procedure or by direct electrophilic substitution of the TTE system. Optical spectroscopy revealed that TTE shows orange emission (470 nm) in a diluted 2-MeTHF matrix at 77 K and blue (420 nm) aggregation-induced emission (AIE) in the solid state. An exhaustive electrochemical study afforded a full rationalization of the electronic properties in terms of the HOMO and LUMO energy levels and gaps, as well as localization and features of the redox centers with respect to TTE functionalization.

Introduction

The interest in organic conjugated molecular systems has grown considerably in recent years owing to their potential use in a great number of different research fields, both fundamental and applied, such as organic light-emitting diodes (OLED),[1] organic field-effect transistors (OFET),[2] and organic photovoltaic devices (OPV).[3] In all these optoelectronic applications, the active organic material plays a crucial role and in general exhibits high effective π-electron delocalization. Nonetheless, although many molecular materials are available, sometimes they suffer from the lack of a versatile synthetic procedure or their properties may be difficult to modulate (e.g., energy gap and shift of the frontier molecular orbital energies). Therefore versatile molecular scaffolds would allow, in principle, a controlled modulation of properties such as absorption/emission and oxidation/reduction potentials through a finely tuned molecular design. In addition, the proper functionalization of the π scaffold may allow control over the solid-state intermolecular interactions and packing.

Well-known and simple molecules such as diphenylethylene (DPE), dithienylethylene (DTE), and tetraphenylethylene (TPE; Figure 1) show interesting optical properties. TPE has been extensively studied because of its tunable luminescent properties and some of its derivatives show the interesting phenomenon of aggregation-induced emission (AIE)[4,5] in which molecules, upon photoexcitation, are not emissive in solution but are strongly luminescent in the solid state.[6,7] Although the thiophene derivative tetra(2-thienyl)ethylene (TTE, Figure 1) could, in principle, be much more appealing than TPE owing to the peculiar electronic properties of the thiophene ring, it has not been as widely studied as TPE. Moreover, regioselective functionalization of the thiophene rings in TTE could lead to the synthesis of a series of derivatives suitable for a systematic electronic, photophysical, and electrochemical investigation. TTE has been known since 1992 and a few TTE derivatives have been reported,[8,9] but no systematic investigations of the structural and electronic features of the TTE class are so far available. Within a wider research project ongoing in our laboratories aimed at investigating different thiophene-based π-conjugated systems for optoelectronic and photovoltaic applications,[10] we have focused our attention on TTE-based molecules as we considered these polyconjugated structures very appealing for the construction of functional molecular materials.

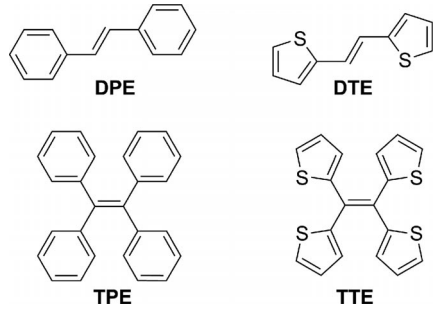

Figure 1. Chemical structures of TTE and related systems.

In this paper we report a new synthetic approach to the preparation of TTE (**1a**) and its derivatives **1b**–**i** (Figure 2), as well as the electrochemical and photophysical characterization of some of them.

[a] Dipartimento di Chimica, Università degli Studi di Milano, Via C. Golgi 19, 20133 Milano, Italy
E-mail: emanuela.licandro@unimi.it
Homepage: http://www.unimi.it
[b] CNR – Istituto di Scienze e Tecnologie Molecolari, via C. Golgi 19, 20133 Milano, Italy
E-mail: clara.baldoli@istm.cnr.it
Homepage: http://www.istm.cnr.it
Supporting information for this article is available on the WWW under http://dx.doi.org/10.1002/ejoc.201300745.

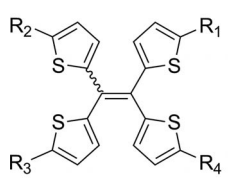

1a $R_1 = R_2 = R_3 = R_4 = H$ **(TTE)**
1b: $R_1 = R_2 = CHO$, $R_3 = R_4 = H$
1c: $R_1 = R_2 = CH_3$, $R_3 = R_4 = H$
1d: $R_1 = R_2 = NO_2$, $R_3 = R_4 = H$
1e: $R_1 = CHO$, $R_2 = R_3 = R_4 = H$
1f: $R_1 = Br$, $R_2 = R_3 = R_4 = H$
1g: $R_1 = R_4 = NO_2$, $R_2 = R_3 = H$
1h: $R_1 = R_2 = R_3 = NO_2$, $R_4 = H$
1i: $R_1 = R_2 = R_3 = R_4 = n$-Bu

Figure 2. Structures of TTE derivatives **1a**–**i**.

Results and Discussion

To date, only two papers have been published concerning the synthesis of TTE (**1a**).[8] In both cases, a McMurry reductive coupling of di(2-thienyl) ketone was used to obtain the product **1a** in about 40% yield, but, in general, this method is not suitable for the synthesis of nonsymmetrically substituted olefins as the coupling between two different carbonyl compounds can lead to a mixture of products. Moreover, some functional groups, such as formyl or halogens, are not compatible with the McMurry reaction conditions. Looking for a solution to these problems, we followed the simple idea of obtaining tetrathienyl-substituted alkenes stereoselectively by a Suzuki–Miyaura cross-coupling reaction between stereodefined *cis*-boronic ester **2** and differently substituted 2-bromothiophenes **3a**–**d** (Scheme 1). We have previously verified the efficiency of this methodology for the one-step synthesis of (*Z*)-1,2-bis(benzodithienyl)ethylenes[11] and we thought that this synthetic method could be an efficient tool for obtaining functionalized TTE systems as the Suzuki–Miyaura reaction exhibits wide functional group compatibility.

The platinum-catalyzed *syn*-diboration of di(2-thienyl)-acetylene **4** (Scheme 1) was performed with bis-pinacolatodiboron in DMF at 150 °C and gave the diboronate **2** as the *Z* isomer. The diboronic ester **2** has already been reported in the literature[12] as an intermediate in the synthesis of thiophene-containing polycyclic aromatic hydrocarbons, but it was neither isolated nor characterized. Although **2** proved to be barely stable in our hands, we succeeded in isolating and fully characterizing it (see the Exp. Sect.). Because of its instability, **2** was then used as a crude intermediate in the subsequent Suzuki–Miyaura cross-coupling reaction with 2.25 equiv. of 2-bromothiophenes **3a**–**d**. The parent TTE (**1a**) was obtained in 50% overall yield and derivatives **1b**, **1c**, and **1d** were obtained, under the same reaction conditions, in yields of 54, 49, and 43%, respectively.

Note that this method is also suitable for the preparation of product **1b** bearing two formyl substituents, which cannot be synthesized by the McMurry procedure.

Considering the stereochemical course of the reaction as reported in the literature,[13] we expected to obtain **1b**–**1d** as the *Z* isomers. However, after chromatographic purification, the ^{1}H NMR (in $CDCl_3$) and HPLC analyses revealed the presence of an almost equimolar *E*/*Z* isomer mixture for **1b** and **1c**, whereas for **1d** the NMR isomer ratio (stereochemistry not assigned) was about 1:2.1. In the case of **1b**, crystals enriched in one of the two isomers were isolated during the chromatographic purification. The ^{1}H NMR spectrum recorded just after the dissolution of such crystals in $CDCl_3$ showed a ratio of 80:20 between the two isomers, but, interestingly, the ^{1}H NMR spectrum recorded on the same sample 6 days later revealed an almost 1:1 isomer ratio, which clearly indicates that an equilibration of the two species takes place in solution. ^{1}H NMR spectra of the dimethyl-substituted TTE **1c** were recorded in different solvents, namely [D_6]DMSO, [D_6]acetone, C_6D_6, and CD_2Cl_2. Compound **1c** is poorly soluble in the more polar solvents, DMSO and acetone, and the spectra recorded of the solutions just after filtration show a ratio of 1:4 of the two isomers in both solvents. After 24 h at room temperature, this ratio was 1:1. In the case of C_6D_6 and CD_2Cl_2, in which compound **1c** is perfectly soluble, the initial ratio of the two isomers was 1:2, but, after 5 h in the case of C_6D_6 and 1 h in the case of CD_2Cl_2, an almost equimolar *E*/*Z* isomer mixture was observed. Therefore the use of the more acidic $CDCl_3$ seems to speed up the equilibration process. As we were interested in studying the unknown reactivity of TTE, we next investigated the direct electrophilic substitution of the thiophene rings. Formylation, bromination, and nitration were performed by using stoichiometric amounts of the electrophile E (Scheme 2).

Vilsmeier formylation was performed by using $POCl_3$ in DMF at 80 °C and gave only the monoformylated compound **1e** in 60% yield, as well as unreacted **1a** (18%). Bromination with *N*-bromosuccinimide (NBS) in DMF at room temperature afforded product **1f** in 50% yield, unreacted **1a** (20%), and a small amount of dibrominated prod-

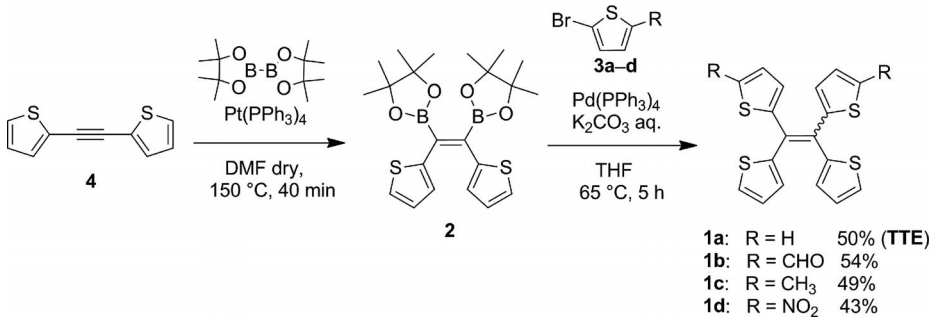

Scheme 1. Synthesis of TTE (**1a**) and its derivatives **1b**–**d**.

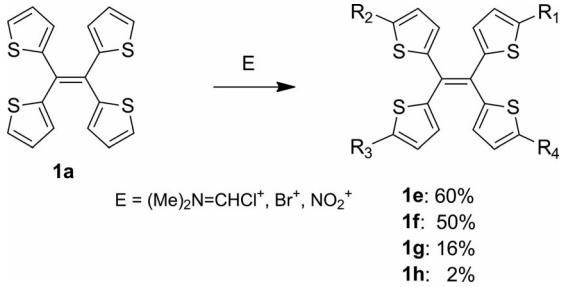

Scheme 2. Electrophilic substitution on TTE.

ucts as a mixture of isomers. The nitration of TTE was attempted following a reported procedure for the mononitration of DTE.[14] A 65% HNO_3 solution (1 equiv.) was slowly added dropwise to a suspension of TTE in acetic acid at room temperature. In this case a mixture of polynitrated compounds was formed from which dinitro **1g** (16%) and trinitro **1h** (2%) derivatives (Figure 2 and Scheme 2) were isolated and completely characterized, as well as unreacted **1a** recovered in 40% yield. Even though the dinitro derivative **1g** was obtained in poor yield, the electrophilic substitution reported in Scheme 2 is interesting as it allows the dinitro derivative **1g**, which is a regioisomer of **1d**, to be obtained.

This novel TTE series is attractive as it allows a detailed optical and electrochemical investigation, the results of which are described below.

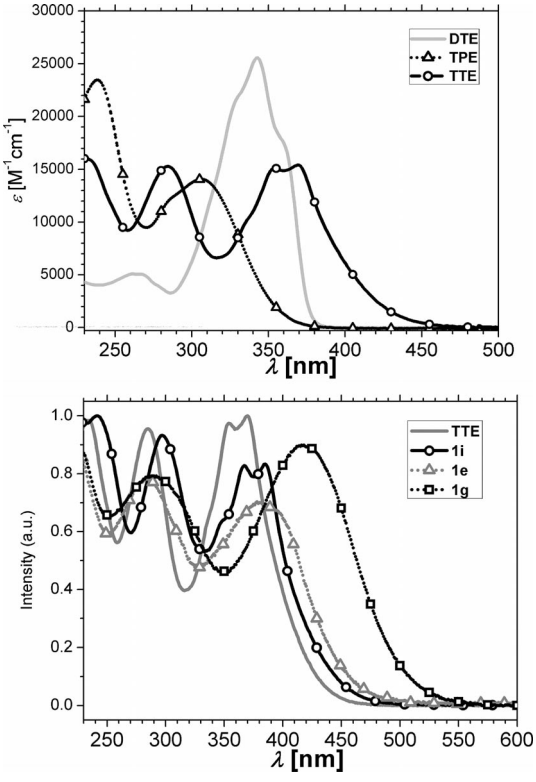

Figure 3. Top panel: Molar absorption spectra of DTE, TPE, and TTE in DCM solution. Bottom panel: Comparative normalized absorption spectra of TTE and its derivatives **1e**, **1g**, and **1i** in DCM solution.

Electronic Spectroscopy

The UV/Vis absorption spectra (Figure 3) and the low-temperature and solid-state emission spectra (Figure 4 and Figure 5) of TTE and some related derivatives are described.

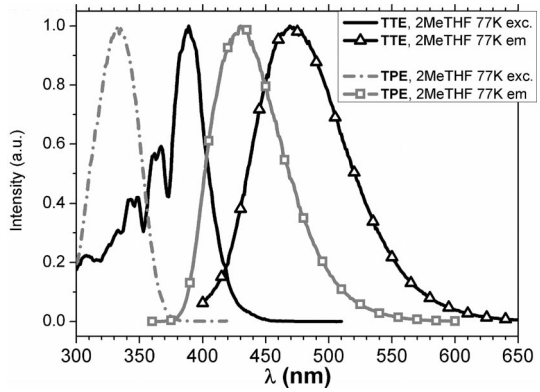

Figure 4. Normalized emission and excitation spectra of TTE (black lines) and TPE (grey lines) in a 2-MeTHF rigid glass at 77 K.

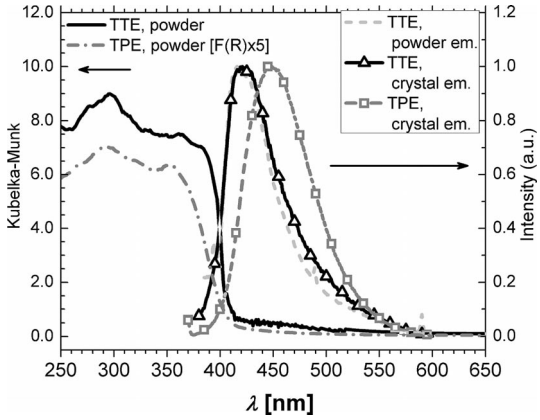

Figure 5. Diffuse reflectance absorption of microcrystalline powders of TTE and TPE (black and grey lines, left axis) and emission spectra of microcrystalline powder and a single crystal of TTE (grey dashed line and black open triangle line respectively) and a TPE single crystal (open squares line).

UV/Vis Absorption Spectra

The absorption spectra of DTE, TPE, and TTE in DCM solution are presented in the top panel of Figure 3. The DTE spectrum displays an absorption maximum at 343 nm (ε = 25550 $M^{-1}cm^{-1}$), which is characterized by a poorly resolved vibronic structure extending up to 380 nm with the lowest-energy peak at 358 nm (optical 0–0 transition, deduced by comparison with the fluorescence of DTE, see below Figure 7). Tetraphenylethylene (TPE) shows two broad unstructured transitions at 240 (ε = 23360 $M^{-1}cm^{-1}$) and 307 nm (ε = 14100 $M^{-1}cm^{-1}$) extending to 370 nm.[15] The optical features of TTE highlight three major transitions at 240 (ε = 15900 $M^{-1}cm^{-1}$), 285 (ε = 15300 $M^{-1}cm^{-1}$), and 370 nm. The lowest-energy band located at 370 nm is characterized by two broad and not fully resolved vibronic

progressions with almost identical molar absorptivity (ε = 15100–15400 $M^{-1} cm^{-1}$) that extend to 450 nm and a shoulder at a shorter wavelength (ca. 335 nm). Therefore TTE displays, in comparison with TPE, a significant redshifted absorption of around 60 nm.

The shape of the low-energy transition of TTE (similar to that of TPE) also indicates that conformational disorder contributes to the spectral broadening of the bands. The functionalization of the TTE scaffold at the α position of the thienyl rings (Figure 3, bottom panel) in the derivatives **1i**, **1g**, and **1e** induces a progressive and constant shift towards lower energies of all the main transitions. In particular, the tetrabutyl derivative **1i**[8b] displays a TTE-like absorption at 384 nm, slightly redshifted by around 15 nm. The monoformylated **1e** and dinitrate **1g** display larger redshifts (the extent of which correlate to the electron acceptor strength and the number of substituents on the conjugated backbone), with absorption maxima at 382 and 420 nm, respectively. Note the loss of the vibrational feature on the lower-energy transition accompanied by band broadening for both **1e** and **1g**.

Low-Temperature Emission Spectra

TTE, analogously to the phenyl-containing TPE, was found to be nonemissive in dilute solutions. The emission spectra of TTE in concentrated DCM solutions, up to saturation, were also recorded, but no luminescence was detected. The intramolecular rotations of the thienyl rings[16] and the twisting of the C=C bond in the excited state are feasible nonradiative relaxation channels for the decay of the excited state (as similarly described for TPE).[4c] In contrast, TTE is highly emissive in a dilute rigid glass of 2-MeTHF at 77 K (Figure 4) and displays a broad featureless fluorescence profile between 420–600 nm with λ_{max} = 470 nm and a full-width half-maxima (FWHM) of 3760 cm^{-1}. The intense emission is likely promoted by the conformational restriction of the molecules in the rigid glass. Therefore the dominating nonradiative relaxation pathways (i.e., intramolecular rotations) in solution at room temperature are depressed in the 77 K rigid matrix. The luminescence excitation profile shows structured progressions at 388, 364, and 345 nm (spaced by ca. 1500 cm^{-1}) that fairly match (even though much sharper in the 77 K experiment) the UV/Vis absorption bands located between 330–430 nm at room temperature. These bands are not sharp, which suggests the possible presence of different conformers even in the glass matrix. The large low-temperature Stokes shift of 4500 cm^{-1} (82 nm), measured from the excitation and emission spectra maxima, and the featureless TTE fluorescence are indicative of a significant excited-state distortion.

The emission and excitation spectra of TPE were measured under the same conditions at 77 K (Figure 4). TPE displays a broad featureless bluish luminescence in the range 380–550 nm with λ_{max} = 430 nm and a FWHM of 3550 cm^{-1}. The TPE luminescence is shifted towards a higher energy by 40 nm relative to TTE; the excitation spectrum mirrors the absorption behavior at room temperature already described. Similarly to TTE, the TPE Stokes shift, 6770 cm^{-1} (100 nm), and its featureless emission suggest analogous significant excited-state distortion.

The absorption and emission spectra of a 2% weight-doped PMMA [poly(methyl methacrylate)] film of TPE and TTE cast onto glass slides were recorded at room temperature (see SI11 in the Supporting Information). The normalized absorptions of the PMMA film of the two compounds perfectly match those of their respective DCM solution, already reported (Figure 3, top panel), which implies no significant intermolecular interactions or observed concentration effects. In the PMMA film, both systems are emissive, similarly to the behavior at 77 K in 2-MeTHF, hence supporting our interpretation that intramolecular rotations are the principal deactivation pathways of the excited states (the emissions are redshifted with respect to the 77 K experiment).

Solid-State Emission Spectra

The absorption profiles of TPE and TTE powders (Figure 5) were recorded in diffuse reflectance mode and plotted in the absorption mode by using the Kubelka–Munk relationship between diffuse reflectance and absorption.[17]

The samples show strong absorption in the range 200–400 nm with three overlapping and poorly resolved bands at 246, 296, and 362 nm. TPE is a well-known conjugated luminogenic compound that displays aggregation-induced emission (AIE) in the solid state. TPE fluoresces in the solid state at 445 nm (Figure 5, grey open-squares line) with a photoluminescent quantum yield (PLQY) of 0.37 and the emission is redshifted by 15 nm compared with the fluorescence at 77 K (Figure 4).

TTE is a white solid, highly emissive both as a microcrystalline powder and as a neat single crystal with a PLQY of 0.06. Surprisingly, aggregated TTE luminesces at about 420 nm (Figure 5, black open triangles line and dashed grey line). Contrary to what would be expected and is found in the case of TPE, TTE emission occurs at an energy 2350 cm^{-1} (50 nm) higher than that of its emission at 77 K. The origin of such a shift[18] could arise from the different structure conformation adopted by TPE and TTE in the solid state.[8a,19] In fact, single-crystal analysis of TPE reveals a propeller like structure in which all of the phenyl rings are twisted, on average, by about 50–55° with respect to the plane describing the ethene double bond.

In contrast, the crystal structure of a known tetramethyl-TTE,[8a] for example, shows that two *trans* thiophene rings adopt a coplanar arrangement and lie on the same plane as the ethene double bond (Figure 6); the other two thiophene rings are almost orthogonal to this plane. The tetramethyl-TTE *trans* coplanar arrangement highlighted in Figure 6 resembles the one adopted by DTE in the crystalline solid (although the intermolecular distances TTE–TTE and DTE–DTE are significantly different).[20] A similar *trans* coplanar conformation is adopted by the tetrakis(mercaptomethyl) derivative of TTE, also reported in ref.[8a] More hindered or bulky substituted TTE structures, like those reported in ref.[9], however, display some torsion

of the thiophene planes with respect to the ethene double bond. The tilting does not exceed 30°, even in the more crowded tetrakis(trimethylsilyl)-TTE derivative of ref.[9a]. However, such molecules are significantly different to TTE; no solid-state PL data are reported to allow useful comparison even though the tetrakis(trimethylsilyl)-TTE is reported to be a white solid similar to TTE.

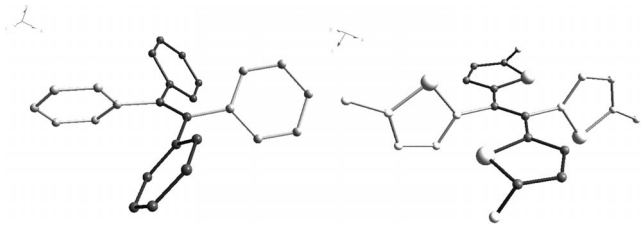

Figure 6. Schematic views of TPE (left) and tetramethyl-TTE (right) molecular conformations in the solid state.

Based on comparisons of the crystal structures and the effective conjugation of π electrons in planar systems with respect to twisted systems, the emissive features of TTE in the solid state would be expected to mirror those of DTE rather than those of TPE. In fact we found that DTE emits in solution (Figure 7) between 380–500 nm with λ_{max} = 400 nm.[21] In the solid state, DTE appears to display two different types of emissive behavior depending on whether it is in its crystalline form (λ_{max} = 438 nm, open triangle) or in the amorphous state (λ_{max} = 420 nm, open squares), as shown in Figure 7.

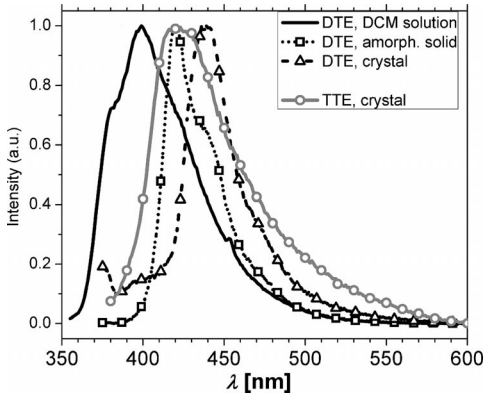

Figure 7. Luminescence emission of DTE in solution (black line), as an amorphous drop-cast film (open squares line), and as a single crystal (open triangle line). Single-crystal TTE emission is overlain for clarity (open circles grey line).

Electrochemical Characterization of TTE Derivatives

A synopsis of normalized voltammetric features obtained in CH_2Cl_2 for the whole series of compounds is shown in the upper panel of Figure 8; the corresponding CV patterns recorded in CH_3CN for the molecules having sufficient solubility in this solvent are presented in the lower panel. The key parameters deduced from peak analysis are collected in Table 1 (CH_2Cl_2) and Table 2 (CH_3CN). Data for the benchmark compounds DTE, DPE, and TPE, obtained under the same conditions, are also reported for the sake of comparison.

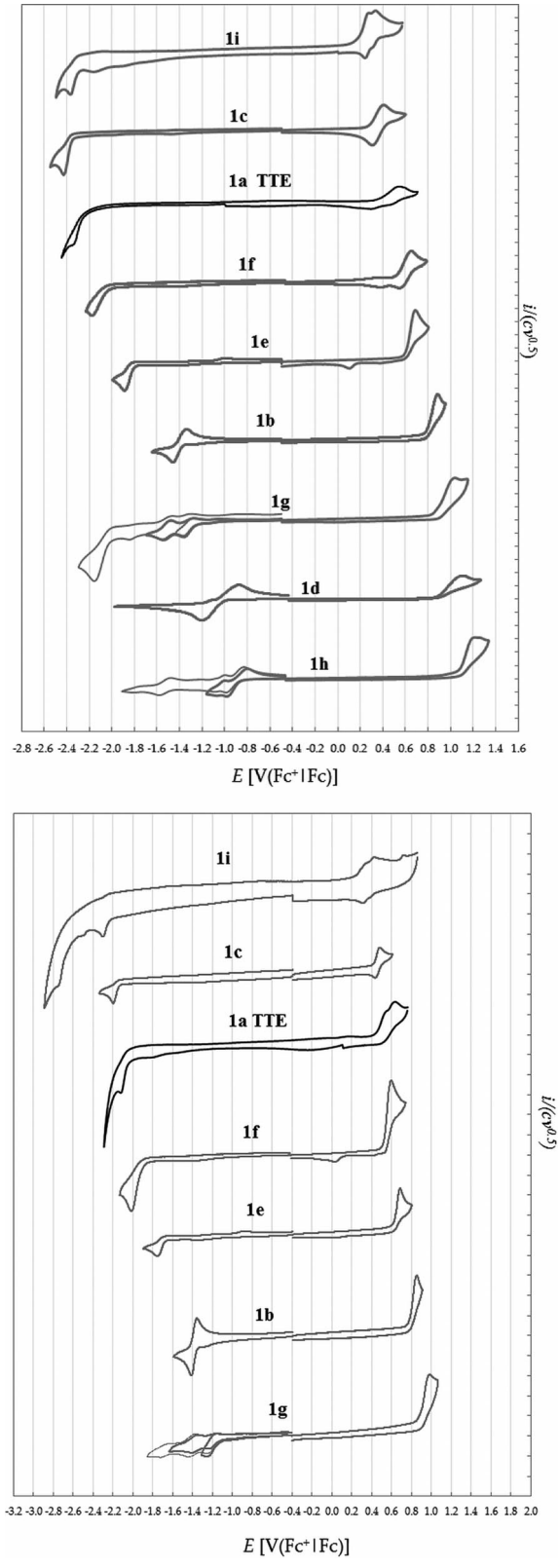

Figure 8. Cyclovoltammograms of the TTE series in CH_2Cl_2 solution (top panel) and CH_3CN (bottom panel) at a scan rate of 0.2 V s^{-1}.

Table 1. Key CV and UV/Vis data for the tetrathienylethylene series and of the reference compounds DTE, DPE, and TPE in CH_2Cl_2 at a scan rate of 0.2 V s^{-1}.

Comp.	$E_{p,Ic}$ [V] (Fc^+|Fc)		$E_{p,Ia}$ [V] (Fc^+|Fc)		LUMO [eV]		HOMO [eV]		HOMO–LUMO gap (CV) [eV]		λ [nm]		HOMO–LUMO gap (optical) [eV]	
	Onset	Max	Onset	Max	Onset	Max	Onset	Max	Onset	Max	Onset	Max	Onset	Max
1a (TTE)	–2.24	–2.32	0.47	0.58	–2.56	–2.48	–5.27	–5.38	2.71	2.90	445	386	2.79	3.21
1b	–1.36	–1.46	0.76	0.89	–3.44	–3.34	–5.56	–5.69	2.12	2.35	488	403	2.54	3.08
1c	–2.12	–2.20	0.41	0.48	–2.68	–2.60	–5.21	–5.28	2.53	2.68	455	372	2.73	3.33
1d	–1.01	–1.20	0.89	1.11	–3.79	–3.60	–5.69	–5.91	1.90	2.31	512	448	2.42	2.77
1e	–1.79	–1.89	0.58	0.70	–3.01	–2.91	–5.38	–5.50	2.37	2.59	483	388	2.57	3.20
1f	–2.05	–2.18	0.52	0.65	–2.75	–2.62	–5.32	–5.45	2.56	2.83	421	372	2.95	3.33
1g	–1.22	–1.36	0.81	1.04	–3.58	–3.44	–5.61	–5.84	2.03	2.40	540	426	2.30	2.91
1h	–0.85	–0.98	1.01	1.21	–3.95	–3.82	–5.81	–6.01	1.87	2.19	538	424	2.31	2.93
1i	–2.25	–2.37	0.18	0.27	–2.55	–2.43	–4.98	–5.07	2.14	2.64	431	370	2.88	3.35
DTE			0.52	0.59			–5.32	–5.39			380	360	3.26	3.45
DPE			0.99	1.08			–5.79	–5.88			335	310	3.70	4.00
TPE			0.82	0.93			–5.62	–5.73			362	305	3.43	4.07

Table 2. Key CV data for the tetrathienylethylene series and of the reference compounds DTE, DPE, and TPE in CH_3CN at a scan rate of 0.2 V s^{-1}.

Comp.	$E_{p,Ic}$ [V] (Fc^+|Fc)		$E_{p,Ia}$ [V] (Fc^+|Fc)		LUMO [eV]		HOMO [eV]		HOMO–LUMO gap (CV) [eV]	
	Onset	Max	Onset	Max	Onset	Max	Onset	Max	Onset	Max
1a (TTE)	–2.06	–2.14	0.47	0.55	–2.74	–2.67	–5.27	–5.35	2.53	2.68
1b	–1.34	–1.41	0.76	0.85	–3.46	–3.39	–5.56	–5.65	2.10	2.27
1c	–2.12	–2.20	0.41	0.48	–2.68	–2.60	–5.21	–5.28	2.53	2.68
1e	–1.68	–1.75	0.60	0.69	–3.13	–3.05	–5.40	–5.49	2.28	2.44
1f	–1.91	–2.02	0.52	0.60	–2.89	–2.78	–5.32	–5.40	2.43	2.62
1i	–2.23	–2.29	0.24	0.35	–2.57	–2.51	–5.04	–5.15	2.47	2.65
DTE	–2.45	–2.56	0.59	0.717	–2.35	–2.25	–5.39	–5.52	3.04	3.27
DPE	–2.59	–2.71	1.02	1.094	–2.21	–2.09	–5.82	–5.89	3.60	3.80
TPE	–2.49	–2.55	0.87	0.992	–2.31	–2.25	–5.67	–5.79	3.36	3.54

Effective Conjugation: TTE Versus TPE Systems

The larger cathodic window available in CH_3CN allows a comparison of both the HOMO and LUMO energy levels as well as the corresponding energy gaps for the DPE/DTE and TPE/TTE analogue pairs, thereby allowing comparison of the effects caused by 1) the replacement of phenyl groups by thiophenes (DPE vs. DTE, TPE vs. TTE) and 2) the presence of four aryl groups rather than two. To this end, a useful scheme is presented in Figure 9 that also includes, as a benchmark, the corresponding data for the T_2, T_3, and T_4 terms in the oligothiophene series.[22]

As already evidenced by Meerholz and Heinze for linear oligomers,[22] it is evident that thiophene systems result in less extreme HOMO and LUMO levels and narrower HOMO–LUMO gaps than the corresponding benzene systems, pointing to higher effective conjugation, and that their HOMO–LUMO gaps decrease much faster with an increasing number of conjugated rings in the thiophene series. In particular, DTE has a higher conjugation efficiency than linear dithiophene T_2, and nearly approaches that of terthiophene, whereas TTE has a higher conjugation efficiency than linear T_4. Because linear oligomers are planar or nearly planar molecules (and for this reason often assumed as benchmarks for effective conjugation), signifi-

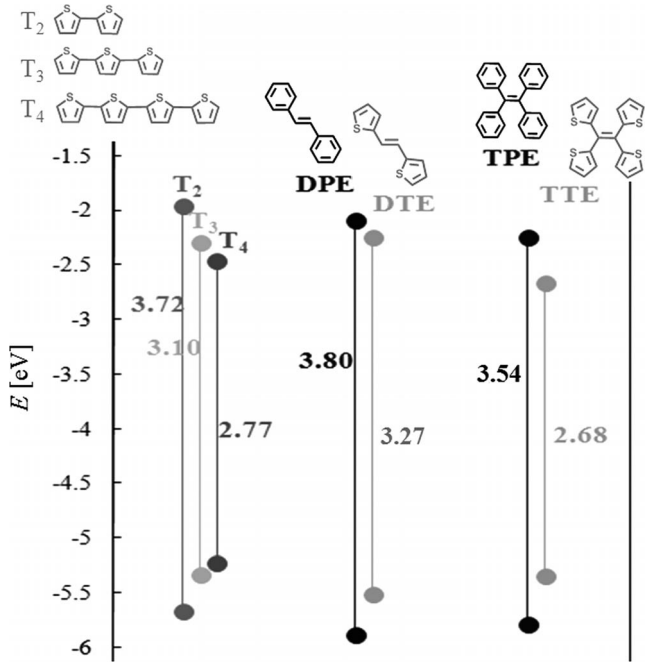

Figure 9. Electrochemical energy gaps for the phenyl and thienyl derivatives.

cant conjugation of the aromatic rings must be assumed for DTE and TTE, together with a significant contribution from the double bond too.

Substituent Effects in the TTE Series

Focusing on the TTE series and looking at Figure 8, at least one oxidation and one reduction peak is perceivable for all the molecules both in CH_2Cl_2 and CH_3CN. The CV patterns regularly shift towards more positive potentials with increasing electron-attracting power of the substituents (from top to bottom). The chemical reversibility of the electron transfer (ET) processes (accounted for by the presence of a symmetrical return peak) regularly improves with the process taking place at increasingly milder potentials (that is, less negative for reductions and less positive for oxidations). In particular, with reference to parent molecule **1a**, weak alkyl electron-donor substituents (**1c** and **1i**) result in a slight shift in the negative direction, which implies a slightly easier oxidation and more difficult reduction. Moreover, the oxidation (unlike the reduction) is chemically reversible, and in the symmetric case **1i** featuring four butyl substituents, two monoelectronic, nearly merging peaks, can be observed (in CH_3CN the same applies also to parent molecule **1a** with four hydrogen substituents), which, according to the literature, can be interpreted in terms of two adjacent cations only weakly interacting for conformational reasons.[8a] Instead, in the case of the dimethyl derivative **1c**, which is an approximately 50:50 *E*/*Z* mixture, only one peak is perceivable. Partial reversibility of the oxidation peak is still observed with the **1f** bromo derivative (in CH_2Cl_2 only). With more powerful electron-attracting groups the oxidation process becomes chemically irreversible, while, symmetrically, the reduction process becomes chemically reversible (**1b**, **1g**, **1d**, **1h**).

In the geminal dinitro case **1g**, two chemically and electrochemically reversible, monoelectronic reduction processes can be perceived, localized on the two nitro groups, which act as equivalent redox centers, that strongly interact, as pointed out by the difference of around 0.2 V between the two peaks. In contrast, the dinitro case **1d**, a mixture of *E* and *Z* isomers, features a wide conjugated system consisting of the central double bond with a nitrothiophene terminal on each side and shows a single, large reduction peak with a symmetrical but distant return peak, which resembles the typical CV response of quinone and quinone-mimic systems (corresponding to a complex combination of electrochemical and chemical steps[23–25]). This feature is indeed worthy of further specific mechanistic investigation. Consistent with **1d** and **1g**, the CV pattern of the trinitro case **1h** appears as the sum of the complex signal corresponding to the above **1d** dinitro conjugated system, and a reversible monoelectronic peak corresponding to the remaining geminal nitro group. All signals are located at more positive potentials, which is consistent with both the higher global electron-attracting inductive effect and improved conjugation.

HOMO and LUMO Energy Levels and Gaps

The HOMO and LUMO energy levels can be calculated from the onset or maximum peak potentials by using Equations (1) and (2).[26,27]

$$E_{LUMO}\ [eV] \approx -1e \times [E_{p\ (or\ onset),Ic}/V(Fc^+|Fc) + 4.8\ V(Fc^+|Fc\ vs.\ zero)] \quad (1)$$

$$E_{HOMO}\ [eV] \approx -1e \times [E_{p\ (or\ onset),Ia}/V(Fc^+|Fc) + 4.8\ V(Fc^+|Fc\ vs.\ zero)] \quad (2)$$

The implications of the two approaches have recently been discussed.[28] A third, more reliable approach, hinging on standard or formal potentials, is not applicable here because it requires all CV peaks considered to be reversible.

The HOMO–LUMO energy gaps calculated from the CV experiments can be compared with those obtained from the UV/Vis absorption spectra (also reported in Table 1), according to Equation (3).

$$E_g\ [eV] = h\ (J\,s) \times c\ (m/s)/[\lambda_{max\ (or\ onset)}\ (m) \times 1.6 \times 10^{-19}\ (J/eV)] \quad (3)$$

Figure 10 shows a good correlation between the two sets of data (particularly calculated by the maxima criterion). Note that the optical gaps are systematically higher than the electrochemical gaps. In fact, the two approaches are not necessarily equivalent because CV implies the production of net charges whereas UV/Vis spectroscopy involves the intramolecular promotion of electrons. Moreover, the two approaches could sometimes involve different energy levels.

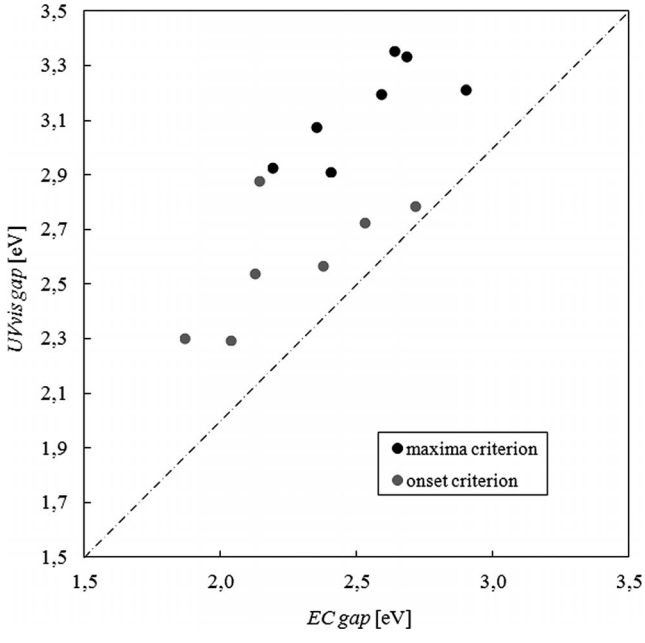

Figure 10. Correlation between the electrochemical (EC) and optical (UV/Vis) energy gaps for compounds **1a**–**c**, **1e**, and **1g**–**i**.

Hammett Correlations

Figure 11 shows that there is an excellent correlation between the electrochemical HOMO and LUMO energy levels and the sums of the Hammett constants[29] of the substituents on the TTE scaffold. Furthermore, the HOMO–LUMO gap consistently decreases with increasing number and electron-withdrawing character of the substituent. This is a consequence of the larger shift to more positive potentials of the reduction process with respect to the oxidation process, which results in the LUMO level decreasing faster than the HOMO level. This observation is consistent with the site of the reduction process being more localized towards the substituent (in particular in the CHO or NO_2 cases) whereas the oxidation should be delocalized over the entire molecular structure. In any case, such rationalization of the molecular energy levels in terms of neat Hammett relationships is a useful feature for target-oriented molecular design in this series.

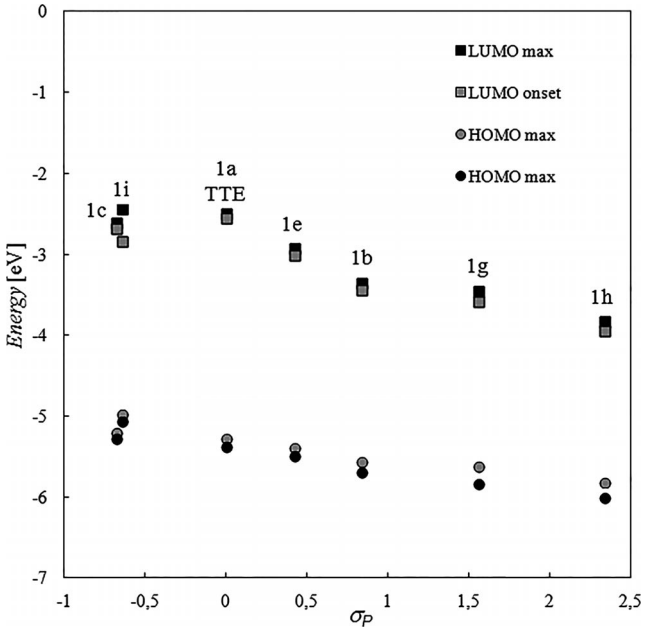

Figure 11. Correlation between electrochemical HOMO and LUMO energy levels and the sums of the corresponding σ_P Hammett constants of the groups substituting TTE in compounds **1a**–**c**, **1e**, and **1g**–**i**.

Solvent Effects

The CV patterns recorded for the same molecule in CH_2Cl_2 and in CH_3CN (Figure 8) appear qualitatively very similar, in terms of both peak morphology (and therefore electron-transfer mechanism) and substituent effects.

However, considering Figure 12 and focusing on the HOMO and LUMO energies in the two solvents, a small but remarkable difference can be perceived. In fact, the HOMO levels almost perfectly coincide, whereas the LUMO levels are slightly but systematically lower in acetonitrile. This could point to the radical-anion intermediate being more stabilized by the polar solvent than the radical cation. This appears to be consistent with the above assumption of the radical anion being more localized than the radical cation.

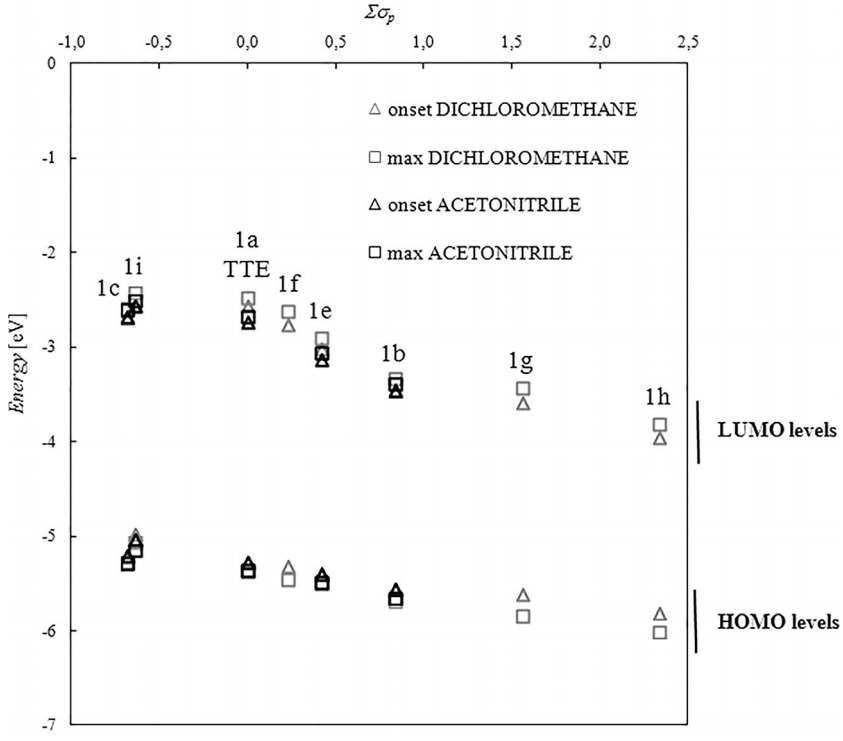

Figure 12. Solvent effect on the Hammett relationships of the electrochemical HOMO and LUMO energy levels of compounds **1a**–**c**, and **1e**–**i**.

Conclusions

This study was driven by the search for new thiophene-based π-conjugated scaffolds for the construction of functional molecular materials and with this aim TTE-based molecules are appealing candidates. We have developed a versatile synthesis of a number of TTE derivatives through a diboration/Suzuki cross-coupling protocol. In addition, the reactivity of TTE towards electrophilic substitution has been tested in nitration, bromination, and formylation reactions.

An extensive electrochemical investigation has been performed on the whole series of compounds, and also on DTE and TPE as benchmarks, resulting in a complete rationalization of the electronic properties, including the HOMO and LUMO energy levels and gaps, and the localization and features of the redox centers in the molecules. Electronic absorption and emission studies were performed on the parent TTE in the solid state and in solution both at room temperature and at 77 K in a rigid 2-MeTHF glass. TTE, which is not luminescent in dilute solution at room temperature, is a bright-orange luminophore in the molecular form at 77 K, emitting at 470 nm. This observation relates to the reduced conformational freedom of the TTE molecules in the rigid glass. Therefore the nonradiative relaxation pathways dominating the behavior in solution at room temperature are reduced in favor of radiative processes in the rigid matrix at 77 K. Two withstanding results of the spectroscopic investigation relate to the fact that 1) TTE displays an AIE (aggregation-induced emission) phenomenon in the neat solid state and 2) the solid-state TTE emission maxima is at 420 nm (blueshifted by 50 nm compared with that at 77 K), which makes it a deep-blue emitter. This shift has been rationalized in terms of a solid-state crystal-packing analysis. In fact, TTE adopts a molecular conformation in which only two of the four thiophenes lie in the same plane as the ethene double bond. Therefore an effective *trans*-DTE-like conjugation dominates the TTE solid-state emission features. Extended ab initio calculations are ongoing in order to support the experimental results and gain a deeper insight into the structure–property relationship of these interesting molecules.

Experimental Section

General: Unless otherwise specified, all the reactions were performed under nitrogen using standard techniques and flasks equipped with a magnetic stirring bar, septum inlet, and reflux condenser. All reagents and solvents were obtained from highest-grade commercial sources and used without further purification. Anhydrous solvents (from Sigma–Aldrich) were purged with nitrogen before use. The reaction outcome was monitored by TLC using silica gel plates and HPLC. All chromatographic separations were carried out on Merck silica gel (60μ, 230–400 mesh). Melting points were obtained with a Büchi B-540 melting point apparatus. ^{1}H and ^{13}C NMR spectra were recorded with Bruker Avance DRX-400, AC300, and AMX 300 MHz spectrometers. The chemical shifts (δ) are reported in parts per million relative to the solvent residual peak ([D$_6$]DMSO, [D$_6$]acetone, CD_2Cl_2, C_6D_6, and $CDCl_3$). UV spectra were recorded by using a Jasco V-520 or Agilent 8453 UV/Vis spectrophotometer in the λ range from 190 to 800 nm at room temperature. UV/Vis diffuse-reflectance spectra were recorded with a Thermo Scientific Evolution 600LC spectrometer equipped with a Praying Mantis Diffuse Reflectance Accessory ($BaSO_4$ was used as 100% reflectance reference). Reflectance data were analyzed by means of the Kubelka–Munk function.[17] Steady-state emission and excitation spectra were measured by using a Horiba Scientific FluoroLog 3 instrument and continuous-wave measurements were obtained with an SPEX 270 M monochromator equipped with an N_2-cooled CCD and a monochromated Xe lamp. The spectra were corrected for the instrument response. The PLQY values for the solid-state materials were obtained by using a home-made integrating sphere and by correcting the spectra of the low-emissive materials for the background of the exciting lamp according to Equation (4) and Equation (5),

$$QY = \frac{P_c^* - (1-A)P_b^*}{AL_a} \quad (4)$$

$$P_{c/b}^* = P_{c/b} - \frac{L_{c/b}}{L_a} P_a \quad (5)$$

in which P and L are the integrated intensities of the PL spectra and the exciting lamp, respectively, index c refers to the measurement with the lamp impinging the sample, and b and a refer to the measurements with the lamp impinging the sphere with the sample inside and outside, respectively, and $A = 1 - L_c/L_b$. Low-temperature measurements were carried out in a 2-MeTHF frozen glass at 77 K. A 2 wt.-% doped PMMA film of the proper chromophore was cast onto glass slides; the chromophore was dissolved in toluene and added to a 100 mg/mL solution of PMMA in toluene to obtain a clear homogeneous solution. HRMS spectra were recorded with a Bruker Daltonics ICR-FTMS APEX II spectrometer. HPLC analyses were performed with an Agilent 1100 series instrument equipped with a PDA detector and a reversed-phase ZORBAX Eclipse XBD-C18 column (4.6× 150 mm, 5 μm particle size) with CH_3CN/H_2O (1 mL/min) as eluent.

***vic*-Bis(pinacolatoboryl)ethylene 2:** Compound **2** was prepared by a slight modification of a reported procedure.[13] A 25 mL flask equipped with a magnetic stirring bar, septum inlet, and a reflux condenser was charged with bis(pinacolato)diboron (250 mg, 1.0 mmol), [Pt(PPh$_3$)$_4$] (20 mg, 0.02 mmol), and dry DMF (2 mL). The mixture was heated at 70 °C and then a solution of di(2-thienyl)acetylene (**4**; 100 mg, 0.53 mmol) in dry DMF (1 mL) was added dropwise. The reaction was heated at 150 °C for 40 min. After distillation of the DMF, the crude *vic*-bis(pinacolatoboryl)ethylene **2** was washed twice with hexane to remove the excess of diboron reagent and then used for the subsequent reaction without any further purification. Crystals of pure **2** were obtained by slow evaporation of a CH_2Cl_2 solution of a crude sample. ^{1}H NMR ($CDCl_3$, 300 MHz): δ = 7.22 (dd, J = 5.1, 1.0 Hz, 2 H), 7.05 (dd, J = 3.5, 1.0 Hz, 2 H), 6.95 (dd, J = 3.5, 5.1 Hz, 2 H), 1.20 (s, 24 H) ppm. ^{13}C NMR ($CDCl_3$, 75 MHz): δ = 126.95, 126.70, 126.35, 125.56, 84.03, 24.70 ppm. ^{11}B NMR ($CDCl_3$, 100 MHz): δ = 30.04 ppm.

General Procedure for the Preparation of Tetrathienylethylenes 1a–d: The crude *vic*-bis(pinacolatoboryl)ethylene **2** (187 mg, 0.42 mmol) was dissolved in THF (3 mL) and the appropriate bromothiophene (0.95 mmol) and [Pd(PPh$_3$)$_4$] (24 mg, 0.02 mmol) were added under vigorous stirring. A solution of 3 M K_2CO_3

(1.1 mL) was added dropwise and the mixture was then heated at reflux for 5 h. After evaporation of the solvent the residue was taken up in CH_2Cl_2 (10 mL). The organic layer was then washed with a saturated solution of NH_4Cl and H_2O, dried, and the solvents evaporated. The crude compounds **1a**–**d** were purified by column chromatography.

Tetra(2-Thienyl)ethylene (1a): Yield 50%. The analytical and spectroscopic data are in agreement with those previously reported.[8]

(*E*/*Z*)-1,2-Bis(5-formyl-2-thienyl)-1,2-di(2-thienyl)ethylene (1b): Yield 54%. R_f = 0.12 (hexane/AcOEt, 9:1). ^{1}H NMR ($CDCl_3$, 300 MHz): Isomer I: δ = 9.81 (s, 2 H), 7.51 (d, J = 4.0 Hz, 2 H), 7.45 (dd, J = 5.0, 1.3 Hz, 2 H), 7.03 (dd, J = 5.0, 3.6 Hz, 2 H), 6.99 (dd, J = 3.6, 1.3 Hz, 2 H), 6.88 (d, J = 4.0 Hz, 2 H) ppm; Isomer II: δ = 9.85 (s, 2 H), 7.58 (d, J = 3.9 Hz, 2 H), 7.38 (dd, J = 5.1, 1.3 Hz, 2 H), 6.98 (d, J = 3.9 Hz, 2 H), 6.96 (dd, J = 5.1, 3.7 Hz, 2 H), 6.91 (dd, J = 3.7, 1.3 Hz, 2 H) ppm. ^{13}C NMR ($CDCl_3$, 75 MHz): δ = 182.92, 144.69, 135.73, 135.18, 131.45, 131.05, 130.63, 128.96, 127.59, 126.99 ppm. UV/Vis (CH_2Cl_2): λ_{max} (ε) = 239 (15766), 311 (16343), 403 (16968), 423 nm (16766 $M^{-1}cm^{-1}$). HRMS (EI): calcd. for $C_{20}H_{12}O_2S_4$ 411.9720; found 411.9713. $C_{20}H_{12}O_2S_4$ (412.55): calcd. C 58.22, H 2.93; found C 57.98, H 2.95.

(*E*/*Z*)-1,2-Bis(5-methyl-2-thienyl)-1,2-di(2-thienyl)ethylene (1c): Yield 49%. R_f = 0.37 (hexane/AcOEt, 9:1). ^{1}H NMR ($CDCl_3$, 300 MHz): Isomer I: δ = 7.34 (dd, J = 5.0, 1.4 Hz, 2 H), 6.97 (dd, J = 5.0, 3.6 Hz, 2 H), 6.94 (dd, J = 3.6, 1.4 Hz, 2 H), 6.67 (d, J = 3.6 Hz, 2 H), 6.59 (dd, J = 3.6, 1.1 Hz, 2 H), 2.40 (br. s, 6 H) ppm; Isomer II: δ = 7.27 (dd, J = 5.1, 1.3 Hz, 2 H), 6.91 (dd, J = 5.1, 3.7 Hz, 2 H), 6.85 (dd, J = 3.7, 1.3 Hz, 2 H), 6.57 (d, J = 3.6 Hz, 2 H), 6.54 (dd, J = 3.6, 1.0 Hz, 2 H), 2.45 (br. s, 6 H) ppm. ^{13}C NMR ($CDCl_3$, 75 MHz): δ = 142.16, 130.00, 129.89, 129.78, 129.67, 127.31, 127.22, 126.66, 126.48, 124.89, 124.73, 15.49, 15.39 ppm. UV/Vis (CH_2Cl_2): λ_{max} (ε) = 230 (15900), 290 (13100), 354 (12160), 370 nm (12450 $M^{-1}cm^{-1}$). HRMS (EI): calcd. for $C_{20}H_{16}S_4$ 384.0135 $[M]^+$; found 384.0143. $C_{20}H_{16}S_4$ (384.59): calcd. C 62.46, H 4.19; found C 62.11, H 4.20.

(*E*/*Z*)-1,2-Bis(5-nitro-2-thienyl)-1,2-di(2-thienyl)ethylene (1d): Yield 43%. R_f = 0.22 (hexane/CH_2Cl_2, 6:4). ^{1}H NMR ($CDCl_3$, 300 MHz): Isomer I: δ = 7.79 (d, J = 4.4 Hz, 2 H), 7.45 (dd, J = 4.9, 1.2 Hz, 2 H), 7.01 (dd, J = 5.0, 3.7 Hz, 2 H), 6.97 (dd, J = 3.7, 1.3 Hz, 2 H), 6.90 (d, J = 4.3 Hz, 2 H) ppm; Isomer II: δ = 7.67 (d, J = 4.4 Hz, 2 H), 7.61 (dd, J = 5.1, 1.2 Hz, 2 H), 7.17 (dd, J = 5.1, 3.6 Hz, 2 H), 7.12 (dd, J = 3.6, 1.1 Hz, 2 H), 6.70 (d, J = 4.4 Hz, 2 H) ppm. ^{13}C NMR ($CDCl_3$, 75 MHz): δ = 153.00, 150.70, 141.64, 139.31, 131.62, 131.20, 130.15, 130.04, 129.87, 129.54, 128.26, 127.48, 127.25 ppm. UV/Vis (CH_2Cl_2): λ_{max} (ε) = 256 (17400), 334 (16350), 434 (21050), 453 nm (20650 $M^{-1}cm^{-1}$). HRMS (EI): calcd. for $C_{18}H_{10}N_2O_4S_4$ 445.9523 $[M]^+$; found 445.9523. $C_{18}H_{10}N_2O_4S_4$ (446.53): calcd. C 48.41, H 2.26, N 6.27; found C 48.69, H 2.24, N 6.29.

1-(5-Formyl-2-thienyl)-1,2,2-tri(2-thienyl)ethylene (1e): Dry DMF (14 μL, 0.18 mmol) was added to a solution of **1a** (50 mg, 0.14 mmol) dissolved in 1,2-dichloroethane (2 mL). The mixture was cooled to 0 °C and $POCl_3$ (16 μL, 0.17 mmol) was added dropwise. The mixture was heated at 80 °C for 8 h. The reaction was then quenched with an aqueous solution of sodium acetate and extracted with CH_2Cl_2 (3× 5 mL). The combined organic layers were washed with H_2O (5 mL), dried with Na_2SO_4, and the solvents evaporated. The crude product was purified by column chromatography (hexane/CH_2Cl_2, 9:1) and **1e** was isolated as a yellow solid in 60% yield. R_f = 0.24 (hexane/AcOEt, 9:1); m.p. 134–135 °C. ^{1}H NMR ($CDCl_3$, 300 MHz): δ = 9.80 (s, 1 H), 7.52 (d, J = 4.0 Hz, 2 H), 7.40 (d, J = 5.0 Hz, 2 H), 7.31 (dd, J = 5.0, 1.2 Hz, 1 H), 7.00 (dd, J = 5.0, 3.7 Hz, 2 H), 6.97 (dd, J = 3.7, 1.2 Hz, 1 H), 6.95 (dd, J = 3.7, 1.2 Hz, 1 H), 6.90 (dd, J = 5.0, 3.7 Hz, 2 H), 6.85 (m, 2 H) ppm. ^{13}C NMR ($CDCl_3$, 75 MHz): δ = 182.98, 155.00, 135.52, 131.22, 130.56, 130.35, 130.27, 129.84, 129.06, 128.88, 128.39, 128.20, 127.61, 127.28, 127.15, 126.95, 126.54 ppm. UV/Vis (CH_2Cl_2): λ_{max} (ε) = 229 (17641), 294 (13796), 388 (12401 $M^{-1}cm^{-1}$). HRMS (EI): calcd. for $C_{19}H_{12}OS_4$ 384.5580 $[M]^+$; found 383.9779. $C_{19}H_{12}OS_4$ (384.54): calcd. C 59.34, H 3.15; found C 59.01, H 3.17.

1-(5-Bromo-2-thienyl)-1,2,2-tri(2-thienyl)ethylene (1f): *N*-Bromosuccinimide (30 mg, 0.17 mmol) was added at room temperature to a stirred solution of **1a** (50 mg, 0.14 mmol) in DMF (2 mL). The reaction was stirred for 24 h at room temperature and then the DMF was removed by distillation in vacuo. The crude mixture was taken up with water (5 mL) and extracted with CH_2Cl_2 (3× 5 mL), the collected organic phases were washed with H_2O (5 mL), dried with Na_2SO_4, and the solvents evaporated. The crude product was purified by column chromatography (hexane/CH_2Cl_2, 8:2) and **1f** was isolated as a pale-yellow solid in 50% yield, together with starting **1a** (20%). R_f = 0.36 (hexane/CH_2Cl_2, 8:2); m.p. 157–159 °C. ^{1}H NMR ($CDCl_3$, 300 MHz): δ = 7.41 (dd, J = 5.0, 1.2 Hz, 1 H), 7.37 (dd, J = 5.0, 1.2 Hz, 1 H), 7.27 (dd, J = 5.0, 1.2 Hz, 1 H), 7.02 (dd, J = 5.0, 3.6 Hz, 1 H), 7.00 (dd, J = 5.0, 3.6 Hz, 2 H), 6.96 (m, 2 H), 6.88 (dd, J = 5.1, 3.7 Hz, 1 H), 6.84 (d, J = 3.9 Hz, 1 H), 6.78 (dd, J = 3.7, 1.2 Hz, 1 H), 6.55 (d, J = 3.9 Hz, 1 H) ppm. ^{13}C NMR ($CDCl_3$, 75 MHz): δ = 145.88, 144.15, 142.87, 142.61, 130.13, 129.46, 129.14, 128.41, 128.02, 127.87, 127.33, 126.99, 126.88, 126.36, 114.83 ppm. UV/Vis (CH_2Cl_2): λ_{max} (ε) = 231 (19860), 286 (12881), 362 nm (13460 $M^{-1}cm^{-1}$). MS (EI): m/z = 434 (^{79}Br) $[M]^+$, 436 (^{81}Br) $[M]^+$. $C_{18}H_{11}B_rS_4$ (435.43): calcd. C 49.65, H 2.55; found C 49.69, H 2.57.

Nitration of TTE: A 65% HNO_3 solution (55 μL, 0.196 mmol) was slowly added dropwise at room temperature to a stirred suspension of **1a** (70 mg, 0.196 mmol) in acetic acid (2 mL). The yellowish suspension turned into an orange-red solution. After 30 min, the reaction was quenched with H_2O (5 mL) and the mixture extracted with CH_2Cl_2 (3× 5 mL). The collected organic phases were washed with $NaHCO_3$ solution (5 mL) and H_2O (2× 5 mL), dried with Na_2SO_4, and the solvents evaporated. The brown residue was purified by column chromatography to afford unreacted **1a** (40%), **1g** (16%) and **1h** (2%).

1,1-Bis(5-nitro-2-thienyl)-2,2-di(2-thienyl)ethylene (1g): Orange solid. R_f = 0.22 (hexane/CH_2Cl_2, 6:4). ^{1}H NMR ($CDCl_3$, 300 MHz): δ = 7.76 (d, J = 4.3 Hz, 2 H), 7.40 (dd, J = 4.7, 1.4 Hz, 2 H), 7.03–6.99 (m, 4 H), 6.85 (d, J = 4.3 Hz, 2 H) ppm. UV/Vis (CH_2Cl_2): λ_{max} (ε) = 229 (19309), 299 (19860), 426 nm (12881 $M^{-1}cm^{-1}$). MS (EI): m/z = 446 $[M]^+$. $C_{18}H_{10}N_2O_4S_4$ (446.53): calcd. C 48.41, H 2.26, N 6.27; found C 48.08, H 2.25, N 6.28.

1,1,2-Tri(5-nitro-2-thienyl)-1-(2-thienyl)ethylene (1h): Orange-brown solid. R_f = 0.16 (hexane/CH_2Cl_2, 1:1). ^{1}H NMR (300 MHz, $CDCl_3$): δ = 7.85 (d, J = 4.3 Hz, 1 H), 7.76 (d, J = 4.3 Hz, 1 H), 7.74 (d, J = 4.3 Hz, 1 H), 7.56 (dd, J = 4.9, 1.3 Hz, 1 H), 7.11–7.05 (m, 2 H), 6.99 (d, J = 4.3 Hz, 1 H), 6.89 (d, J = 4.3 Hz, 1 H), 6.85 (d, J = 4.3 Hz, 1 H) ppm. UV/Vis (CH_2Cl_2): λ_{max} (ε) = 228 (19891), 308 (16643), 424 nm (17760 $M^{-1}cm^{-1}$). MS (EI): m/z = 491 $[M]^+$. $C_{18}H_9N_3O_6S_4$ (491.53): calcd. C 43.98, H 1.85; found C 43.91, H 1.86.

Tetrakis(5-butyl-2-thienyl)ethylene (1i): Yield 20%. Yellow solid. Synthesized according to a literature procedure.[8a] The analytical and spectroscopic data are in agreement with those previously reported.[8b]

Electrochemistry: All compounds were studied by cyclovoltammetry at scan rates typically in the range 0.05–2 $V s^{-1}$. The concentration of the substrates was typically 0.0005 M in CH_2Cl_2 and in CH_3CN with 0.1 M tetrabutylammonium hexafluorophosphate ($TBAPF_6$) as the supporting electrolyte. The solutions were deaerated by N_2 bubbling. The ohmic drop was compensated by the positive feedback technique.[30]

The experiments were performed with an AUTOLAB PGSTAT potentiostat (EcoChemie, The Netherlands) run by a PC with GPES software. The working electrode was a glassy carbon (GC) electrode (AMEL, diameter = 1.5 mm) cleaned with diamond powder (Aldrich, diameter = 1 μm) on a wet cloth (Struers DP-Nap). The counter electrode was a platinum wire, while the reference electrode was an aqueous saturated calomel electrode (SCE), having – vs. the $Fc^+|Fc$ couple (the intersolvental redox potential reference currently recommended by IUPAC)[31,32] – a difference of –0.495 V in CH_2Cl_2 and of –0.391 V in CH_3CN.

Supporting Information (see footnote on the first page of this article): Additional UV/Vis, NMR and mass spectra, HPLC traces, and cyclic voltammograms.

Acknowledgments

The authors gratefully acknowledge Prof. Stefano Maiorana for helpful discussions and Dr. Chiara Botta and Dr. Francesca Villafiorita Monteleone of the ISMAC-CNR of Milan for PLQY measurements. This work was supported by the Università degli Studi di Milano and the National Research Council, Italy (project CNR-PMP04.012.002)

[1] S. J. Dhobleb, N. T. Kalyania, *Renewable Sustainable Energy Rev.* **2012**, *16*, 2696–2723.
[2] G. M. Farinola, A. Operamolla, *Eur. J. Org. Chem.* **2011**, 423–450.
[3] C. W. Schlenker, M. E. Thompson, *Top. Curr. Chem.* **2012**, *312*, 175–212.
[4] a) N. B. Shustova, B. D. McCarthy, M. Dinča, *J. Am. Chem. Soc.* **2011**, *133*, 20126–20129; b) Y. Xu, L. Chen, Z. Guo, A. Nagai, D. Jiang, *J. Am. Chem. Soc.* **2011**, *133*, 17622–17625; c) F. Mahtab, J. W. Y. Lam, J. Liu, W. Yuan, P. Lu, B. Z. Tang, *Small* **2011**, *7*, 1448–1455.
[5] a) Y. Hong, J. W. Y. Lam, B. Z. Tang, *Chem. Soc. Rev.* **2011**, *40*, 5361–5388; b) Z. Zhao, J. W. Y. Lam, B. Z. Tang, *Curr. Org. Chem.* **2010**, *14*, 2109–2132; c) Y. Hong, J. W. Y. Lam, B. Z. Tang, *Chem. Commun.* **2009**, 4332–4353.
[6] a) Z. Chi, X. Zhang, B. Xu, X. Zhou, C. Ma, Y. Zhang, S. Liua, J. Xu, *Chem. Soc. Rev.* **2012**, *41*, 3878–3896; b) N.-W. Tseng, J. Liu, J. C. Y. Ng, J. W. Y. Lam, H. H. Y. Sung, I. D. Williams, B. Z. Tang, *Chem. Sci.* **2012**, *3*, 493–497; M. Wang, G. Zhang, D. Zhang, D. Zhu, B. Z. Tang, *J. Mater. Chem.* **2010**, *20*, 1858–1867.
[7] a) W. Wang, T. Lin, M. Wang, T. X. Liu, L. Ren, D. Chen, S. Huang, *J. Phys. Chem. B* **2010**, *114*, 5983–5988; b) A. Qin, J. W. Y. Lam, B. Z. Tang, *Prog. Polym. Sci.* **2012**, *37*, 182–209.
[8] a) T. Suzuki, H. Shioara, M. Monobe, T. Sakimura, S. Tanaka, Y. Yamashita, T. Miyashi, *Angew. Chem.* **1992**, *104*, 454; *Angew. Chem. Int. Ed. Engl.* **1992**, *31*, 455–458; b) E. Fischer, J. Larsen, J. B. Christensen, M. Fourmigue, H. G. Madsen, N. Harrit, *J. Org. Chem.* **1996**, *61*, 6997–7005.
[9] a) T. Wu, J. Shi, C. Li, J. Song, L. Xu, H. Wang, *Org. Lett.* **2013**, *15*, 354–357; b) H. Halvorsen, J. Skramstad, H. Hope, *Synth. Commun.* **2007**, *37*, 1179–1187.
[10] a) E. Longhi, A. Bossi, S. Maiorana, G. Di Carlo, F. De Angelis, P. Salvadori, A. Petrozza, M. Binda, V. Roiati, P. R. Mussini, C. Baldoli, E. Licandro, *Eur. J. Org. Chem.* **2013**, *1*, 84–94; b) S. Maiorana, E. Licandro, E. Longhi, S. Cauteruccio, A. Abbotto, C. Baldoli, F. De Angelis, PCT Int. Appl., WO 2012107488 A2 20120816, **2012**; c) S. Maiorana, E. Licandro, E. Longhi, C. Baldoli, F. De Angelis, Italian Patent Appl. MI2011A000184, **2011**; d) C. Kim, T. J. Marks, A. Facchetti, M. Schiavo, A. Bossi, S. Maiorana, E. Licandro, F. Todescato, S. Toffanin, M. Muccini, C. Graiff, A. Tiripicchio, *Org. Electron.* **2009**, *10*, 1511–1520; e) A. Bossi, L. Falciola, C. Graiff, S. Maiorana, C. Rigamonti, A. Tiripicchio, E. Licandro, P. R. Mussini, *Electrochim. Acta* **2009**, *54*, 5083–5097; f) S. U. Giovannella, C. Botta, A. Bossi, E. Licandro, S. Maiorana, *J. Appl. Phys.* **2006**, *100*, 083107.
[11] C. Baldoli, A. Bossi, C. Giannini, E. Licandro, S. Maiorana, D. Perdicchia, M. Schiavo, *Synlett* **2005**, 1137–1141.
[12] a) M. Shimizu, I. Nagao, Y. Tomioka, T. Kadowaki, T. Hiyama, *Tetrahedron* **2011**, *67*, 8014–8026; b) M. Shimizu, I. Nagao, Y. Tomioka, T. Kadowaki, T. Hiyama, *Angew. Chem.* **2008**, *120*, 8216; *Angew. Chem. Int. Ed.* **2008**, *47*, 8096–8099.
[13] a) T. Ishiyama, N. Matsuda, M. Murata, F. Ozawa, A. Suzuki, N. Miyaura, *Organometallics* **1996**, *15*, 713–720; b) H. Prokopcová, J. Ramírez, E. Fernández, O. Kappe, *Tetrahedron Lett.* **2008**, *49*, 4831–4835.
[14] M. H. Garcia, P. Florindo, M. F. M. Piedade, M. T. Duarte, M. P. Robalo, E. Goovaertis, W. Wenseleers, *J. Organomet. Chem.* **2009**, *694*, 433–445.
[15] Y. Dong, J. W. Y. Lam, A. Qin, J. Liu, Z. Li, *Appl. Phys. Lett.* **2007**, *91*, 011111.
[16] a) S. Sharafy, K. A. Muszkat, *J. Am. Chem. Soc.* **1971**, *93*, 4119–4125; b) D. A. Shultz, M. A. Fox, *J. Am. Chem. Soc.* **1989**, *111*, 6311–6320.
[17] $F(R) = \frac{(1-R)^2}{2R} = \frac{k}{s}$, in which R = measured reflectance value, k = absorption coefficient, and s = scattering coefficient.
[18] Y.-X. Li, H.-B. Zhou, J.-L. Miao, G.-X. Sun, G.-B. Li, Y. Nie, C.-L. Chen, Z. Chen, X.-T. Tao, *CrystEngComm* **2012**, *14*, 8286–8291.
[19] a) A. Hoekstra, A. Vos, *Acta Crystallogr., Sect. B: Struct. Sci.* **1975**, *31*, 1716–1721; b) G. Hua, Y. Li, A. M. Z. Slawin, J. D. Woollins, *Dalton Trans.* **2007**, 1477–1480; c) I. Ino, L. P. Wu, M. Munakata, T. Kuroda-Sowa, M. Maekawa, Y. Suenaga, R. Sakai, *Inorg. Chem.* **2000**, *39*, 5430–5436.
[20] G. Ruban, D. Zobel, *Acta Crystallogr., Sect. B: Struct. Sci.* **1975**, *31*, 2632–2635.
[21] a) G. Neculqueo, V. Rojas Fuentes, A. Lòpez, R. Matute, S. O. Vàsquez, F. Martìnez, *Struct. Chem.* **2012**, *23*, 1751–1760; b) T. Itoh, M. Yamaji, *J. Phys. Chem. A* **2008**, *112*, 13413–13418.
[22] K. Meerholz, J. Heinze, *Electrochim. Acta* **1996**, *41*, 1839–1854.
[23] M. A. Bhat, *Electrochim. Acta* **2012**, *81*, 275–282.
[24] E. Laviron, *J. Electroanal. Chem.* **1984**, *164*, 213–227.
[25] E. Laviron, *J. Electroanal. Chem.* **1984**, *169*, 29–46.
[26] W.-Y. Wong, X.-Z. Wang, Z. He, A. B. Djurisic, C.-T. Yip, K.-Y. Cheung, H. Wang, C. S. K. Mak, W.-K. Chan, *Nat. Mater.* **2007**, *6*, 521–527.
[27] R. S. Ashraf, M. Shahid, E. Klemm, M. Al-Ibrahim, S. Sensfuss, *Macromol. Rapid Commun.* **2006**, *27*, 1454–1459.
[28] R. Po, M. Caldararo, S. Chiaberge, L. Gila, L. Longo, P. R. Mussini, A. Pellegrino, N. Perin, M. Salvalaggio, A. Savoini, S. Spera, *Electrochim. Acta* **2011**, *56*, 6638–6653.
[29] C. Hansch, A. Leo, R. W. Taft, *Chem. Rev.* **1991**, *91*, 165–195.
[30] A. J. Bard, L. R. Faulkner, in: *Electrochemical Methods. Fundamentals and Applications*, 2nd ed. Wiley, New York, **2001**, p. 648–650.
[31] G. Gritzner, J. Kuta, *Pure Appl. Chem.* **1984**, *56*, 461.
[32] G. Gritzner, *Pure Appl. Chem.* **1990**, *62*, 1839.

Received: May 21, 2013
Published Online: August 28, 2013

